Atom Indonesia

Journal homepage: http://atomindonesia.brin.go.id

# Effect of $MoO_3$ on the Radiation Shielding Properties of Bismuth Boro-Tellurite Glass ($B_2O_3$-$TeO_2$-$Bi_2O_3$-$Li_2O$): Theoretical and Simulation Studies

**O. A. Putra[1*], R. H. Asiah[2], H. Sutanto[1], S. Faniandari[1], E. B. Yutomo[1]**

[1]*Department of Physics, Faculty of Science and Mathematics, Diponegoro University, Semarang, 50275, Indonesia*
[2]*Department of Radiology, dr. Kariadi Central General Hospital, Semarang, 50244, Indonesia*

**ARTICLE INFO**

*Article history:*
Received 17 January 2025
Received in revised form 1 October 2025
Accepted 1 December 2025

*Keywords:*

Bismuth boro-tellurite glass
Radiation shielding
XCOM
Phy-X/PSD
Interaction of radiation with matter

**ABSTRACT**

This study aims to evaluate the efficiency of bismuth boro-tellurite glass modified with molybdenum oxide ($MoO_3$) as a gamma-ray shielding material in the (50-x)$B_2O_3$-10$TeO_2$-30$Bi_2O_3$-10$Li_2O$-x$MoO_3$ (x = 0, 4, 8, 12, and 16 mol%) glass system. Five designed compositions (x = 0-16 mol%) were evaluated over 0.01-15 MeV using XCOM (NIST) and Phy-X/PSD for derived shielding metrics. The calculation results from both programs agreed closely with a maximum difference of only 0.037%, confirming numerical consistency of MAC across tools. Estimated glass density increased with $MoO_3$ content from 5.666 to 5.948 g/cm$^3$ (BBTM1 to BBTM5), which raised LAC and improved thickness indicators. The results showed that at 0.05 MeV the highest LAC was recorded for BBTM5 (38.085 cm$^{-1}$) compared with BBTM1-BBTM4 (35.364-37.409 cm$^{-1}$), and at 1.00 MeV the HVL decreased from 1.789 cm (BBTM1) to 1.736 cm (BBTM5). Sample BBTM5, with the highest $MoO_3$ concentration, consistently exhibited higher LAC and larger $Z_{eff}/N_{eff}$ across energies, and a lower Transmission Factor (TF) across representative radioisotope energies (0.662-2.506 MeV), indicating superior gamma-ray shielding effectiveness.



## INTRODUCTION

Radiation shielding made of concrete mixed with lead has long been used as a common solution for gamma-ray protection [1]. However, this material has a number of significant drawbacks, such as high porosity, low thermal and chemical stability, poor structural homogeneity, and shrinkage cracking [2]. These drawbacks directly reduce its effectiveness as a radiation shield. In addition, concrete-based shielding materials require large thicknesses, making them difficult to apply to systems with limited space [3]. The use of lead as a shielding material is also a serious concern due to its toxic properties that can endanger the health of workers and potentially pollute the environment [4,5].

To overcome these limitations, researchers are looking for safer and more effective alternative radiation shielding materials. One promising alternative is the use of glass as a radiation shield. Glass shields have several advantages, including optical transparency that allows radiation workers to visually observe objects without the risk of direct exposure to radiation [6,7]. In addition, the flexible nature of glass allows its application in confined spaces, making it a practical choice in a variety of conditions [8]. Good thermal stability, relatively low production costs, environmentally friendly properties due to recyclability, and non-toxicity make it a safe and sustainable alternative for radiation protection [9,10].

Borate glass (boron oxide-based glass) has advantages in terms of lower formation temperature (~260°C) and melting temperature (~450°C) compared to silicate glass, which is in the range of

*Corresponding author.
E-mail address: Okiadep@fisika.fsm.undip.ac.id
DOI: https://doi.org/10.55981/aij.2026.1616

1100°C and 1728°C, respectively [11]. Similar things are also found in telluride glass (tellurium oxide-based glass), which has a relatively low melting temperature (~700°C), high density, and good mechanical strength. The use of materials with lower processing temperatures not only supports energy efficiency but also has the potential to reduce the production cost of glass-based radiation shields significantly. Bismuth boro-tellurite glass is one type of glass that has great potential as a future radiation shield. This type of glass contains a mixture of bismuth oxide, boron oxide, and tellurium oxide, each of which contributes unique and synergistic properties that increase the effectiveness of the material as a radiation shield. The combination of these three components is able to provide good thermal and chemical stability properties [12], superior optical properties [13], and impressive mechanical properties [14]. Previous studies have shown a positive trend towards the addition of transition metals to improve the quality of bismuth boro-tellurite glass as a radiation shielding material. A study conducted by S. M. Ngaram et al. (2025) evaluated the effect of adding tungsten oxide ($WO_3$) to bismuth boro-tellurite glass with a molecular composition of (70-x)$B_2O_3$-5$TeO_2$-10$Bi_2O_3$-10$SrCO_3$-5$K_2CO_3$-x$WO_3$ [15]. The results of this study indicate that increasing the concentration of WO3 can increase the material's ability to absorb radiation.

Another study conducted by M. S. Al-Buriahi et al. (2024) also investigated the effect of increasing the concentration of molybdenum oxide ($MoO_3$) on cadmium zinc lithium-borate glass with a composition of 60$B_2O_3$-20CdO-10ZnO-(10-x)$Li_2O$-x$MoO_3$ (x = 0, 0.5, 1.0, 1.5, and 2.0 mol%) [16]. The results of this study prove that the addition of $MoO_3$ significantly increases the supporting parameters of radiation protection, such as density, Mass Attenuation Coefficient (MAC), Linear Attenuation Coefficient (LAC), Effective Atomic Number ($Z_{eff}$), and Effective Electron Density ($N_{eff}$), which strengthens the ability of this glass as a radiation shield. Transition metal oxides such as $MoO_3$ have unique properties in improving the quality of glass because Mo turns into $Mo^{6+}$ ions, which contribute to the absorption of radiation energy and material stability. However, research on the effect of adding $MoO_3$ on the quality of bismuth boro-tellurite glass as a radiation shield has yet to be widely conducted.

This study evaluates the efficiency of bismuth boro-tellurite glass with MoO3 as a radiation shield in the 0.01-15 MeV range. Shielding parameters were calculated using XCOM (NIST) and Phy-X/PSD, integrating cross-section data with practical metrics. XCOM validates photon cross sections and Mass Attenuation Coefficients (MAC) for elements, compounds, or mixtures based on elemental composition over 1 keV-100 GeV [17]. Phy-X/PSD is an online platform that calculates MAC and additional shielding metrics, including Half-Value Layer (HVL), Tenth-Value Layer (TVL), Mean Free Path (MFP), effective atomic number (Zeff), and electron density (Neff), across a similar range [18]. XCOM supplies validated cross-section and MAC data, while Phy-X/PSD rapidly provides practical shielding indicators for benchmarking glass compositions before experiments. Both tools were selected for their complementary strengths.

## THEORY

Linear Attenuation Coefficient (LAC, μ) can be calculated based on the Beer-Lambert law [19]. To evaluate the radiation attenuation capability per unit mass of the shielding material, the Mass Attenuation Coefficient (MAC) is calculated by dividing the LAC value by the density of the shielding material [20]. MAC measures the fraction of photons removed from the ionizing radiation beam by the shielding material per unit mass. The MAC value of the radiation shielding is as in Eq. (1).

$$MAC = \frac{\mu}{\rho} = \sum_i w_i \left(\frac{\mu}{\rho}\right)_i \quad (1)$$

Half-Value Layer (HVL) is the thickness of the shielding material required to reduce the radiation intensity to half of its original intensity and can be calculated using Eq. (2). Meanwhile, the Tenth-Value Layer (TVL) is the thickness of the shielding material required to reduce the radiation intensity to 10% of its original intensity and can be calculated using Eq. (3) [3,21].

$$HVL = \frac{\ln 2}{\mu} \quad (2)$$

$$TVL = \frac{\ln 10}{\mu} \quad (3)$$

The Mean Free Path (MFP) is the inverse of the linear attenuation coefficient and represents the average distance a photon or particle of radiation can travel in a material without experiencing interaction, as expressed in Eq. (4) [22].

$$MFP = \frac{1}{\mu} \quad (4)$$

Effective Atomic Number ($Z_{eff}$) is a parameter that indicates the ability of a material to interact with ionizing radiation based on its constituent elements. The $Z_{eff}$ value describes the reactivity of the material to radiation, depending on the

composition of elements with different atomic numbers. The equation for calculating $Z_{eff}$ can be found by calculating the ratio between the total atomic cross-section ($\sigma_a$) and the total electronic cross-section ($\sigma_e$), as given in Eq. (5) [23,24]:

$$Z_{eff} = \frac{\sigma_a}{\sigma_e} = \frac{\sum_i f_i A_i \left(\frac{\mu}{\rho}\right)_i}{\sum_i f_i \frac{A_j}{Z_j}\left(\frac{\mu}{\rho}\right)_j} \quad (5)$$

Where, $f_i$, A, and Z are the molar fraction, atomic mass per mole, and atomic number of the i-th element in the component, respectively.

Effective Electron Density ($N_{eff}$) is the number of effective electrons as the main component in the radiation absorption process per unit mass of material that is able to interact with ionizing radiation, and can be evaluated using Eq. (6) [25].

$$N_{eff} = N_A \frac{Z_{eff}}{\sum_i f_i A_i} \quad (6)$$

Transmission Factor (TF) is measured as the proportion of photons that successfully pass through the shielding material, as defined in Eq. (7) [26].

$$TF = \left(\frac{I}{I_0}\right) \times 100\ \% = e^{-\mu t} \times 100\ (\%) \quad (7)$$

TF is calculated with thickness variations (t = 0.5-3 cm), in accordance with the energy commonly used in radioisotopes, namely 0.662 ($^{137}$Cs), 1.173 ($^{60}$Co), 1.332, and 2.506 ($^{60}$Co) MeV to make it consistent with Fig. 6 and the related text.

## METHODS

The chemical composition of five samples of bismuth boro-tellurite glass modified $MoO_3$ has a molecular formula of (50-x)$B_2O_3$-10$TeO_2$-30$Bi_2O_3$-10$Li_2O$-x$MoO_3$, with x values of 0, 4, 8, 12, and 16 mol%. The sample codes are BBTM1, BBTM2, BBTM3, BBTM4, and BBTM5, respectively. Table 1 shows the chemical composition of each sample and the corresponding theoretical density estimates [27,28].

This is a theoretical/simulation study; no physical glass samples (BBTM1-BBTM5) were fabricated. The designed compositions were used for computational evaluation of photon-interaction and shielding parameters consistent with the Theory section.

Oxide contents (mol%) were converted to oxide mass fractions using molar masses. Each oxide was then decomposed stoichiometrically into its constituent elements (B, O, Te, Bi, Li, Mo). Elemental masses were summed over all oxides and renormalized to obtain elemental weight fractions ($w_B$, $w_O$, $w_{Te}$, $w_{Bi}$, $w_{Li}$, and $w_{Mo}$) required by XCOM/Phy-X/PSD. This procedure defines the input composition for photon-interaction calculations [29] and ensures consistency with Eq. (1).

The glass density for each designed composition was estimated using the additive specific-volume / inverse rule-of-mixtures approach commonly applied to multi-oxide glasses, as expressed in Eq. (8).

$$\rho_{glass} = \frac{\sum_i n_i M_i}{\sum_i \frac{n_i M_i}{\rho_i}} \text{ or equivalently } \frac{1}{\rho_{glass}} = \sum_i \frac{w_i}{\rho_i} \quad (8)$$

where $n_i$ is the mole amount of oxide *i*, $M_i$ *is* its molar mass, $\rho_i$ is the bulk density of the pure oxide, and $w_i$ is the mass fraction of oxide *i*. This additive-volume form is standard for oxide glasses and yields reliable estimates when $\rho_i$ values are taken from accredited compilations [28]. The resulting $\rho_{glass}$ was then used to convert MAC to LAC and to compute HVL, TVL, and MFP as in Eqs. (2-4).

Based on the data in Table 1, lithium (Li) has the lowest weight percentage in all $MoO_3$-modified bismuth boro-tellurite glasses, while oxygen (O) shows the highest weight percentage. The molybdenum (Mo) element is absent in the first sample (x = 0) and increases progressively from the second (x = 4 mol%) to the fifth (x = 16 mol%). Figure 1 shows a monotonic increase in the estimated density with $MoO_3$ content, consistent with substituting heavier/higher-$\rho$ oxide and reducing lighter $B_2O_3$/$Li_2O$ fractions.

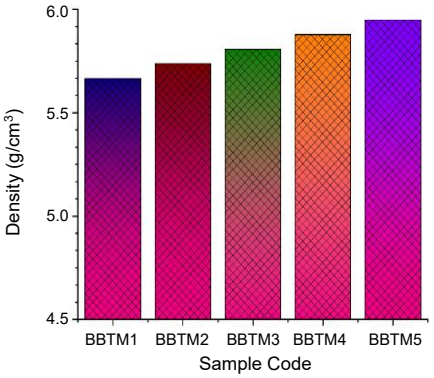


**Fig. 1.** Density variation of $MoO_3$-based glasses (g/cm³).

**Table 1.** Fraction weight of the component (wt.%) and theoretical density estimates of each sample.

| Sample | | Li | B | O | Mo | Te | Bi | Density |
|---|---|---|---|---|---|---|---|---|
| BBTM1 | 50$B_2O_3$-10$TeO_2$-30$Bi_2O_3$-10$Li_2O$-0$MoO_3$ | 0.00717 | 0.05585 | 0.22319 | 0 | 0.06592 | 0.64784 | 5.666 |
| BBTM2 | 46$B_2O_3$-10$TeO_2$-30$Bi_2O_3$-10$Li_2O$-4$MoO_3$ | 0.00706 | 0.05061 | 0.21981 | 0.01952 | 0.06493 | 0.63804 | 5.737 |
| BBTM3 | 42$B_2O_3$-10$TeO_2$-30$Bi_2O_3$-10$Li_2O$-8$MoO_3$ | 0.00695 | 0.04552 | 0.21654 | 0.03847 | 0.06396 | 0.62854 | 5.808 |
| BBTM4 | 38$B_2O_3$-10$TeO_2$-30$Bi_2O_3$-10$Li_2O$-12$MoO_3$ | 0.00685 | 0.04058 | 0.21336 | 0.05686 | 0.06302 | 0.61931 | 5.878 |
| BBTM5 | 34$B_2O_3$-10$TeO_2$-30$Bi_2O_3$-10$Li_2O$-16$MoO_3$ | 0.00675 | 0.03578 | 0.21027 | 0.07472 | 0.06211 | 0.61034 | 5.948 |

**Table 2.** Mass Attenuation Coefficients (MAC) ($cm^2/g$) from XCOM and Phy-X/PSD for BBTM1-BBTM5, with percent deviation (%) at selected energies.

| Energy (MeV) | BBTM1 | | | BBTM2 | | | BBTM3 | | | BBTM4 | | | BBTM5 | | |
|---|---|---|---|---|---|---|---|---|---|---|---|---|---|---|---|
| | XCOM | Phy-X | Δ (%) | XCOM | Phy-X | Δ (%) | XCOM | Phy-X | Δ (%) | XCOM | Phy-X | Δ (%) | XCOM | Phy-X | Δ (%) |
| 0.010 | 99.400 | 99.404 | 0.004 | 99.570 | 99.569 | 0.001 | 99.730 | 99.730 | 0.000 | 99.890 | 99.885 | 0.005 | 100.000 | 100.037 | 0.037 |
| 0.015 | 78.910 | 78.910 | 0.001 | 78.270 | 78.272 | 0.002 | 77.650 | 77.652 | 0.003 | 77.050 | 77.051 | 0.001 | 76.470 | 76.467 | 0.004 |
| 0.020 | 59.750 | 59.745 | 0.008 | 60.390 | 60.394 | 0.006 | 61.020 | 61.023 | 0.004 | 61.630 | 61.633 | 0.005 | 62.230 | 62.226 | 0.006 |
| 0.030 | 21.030 | 21.034 | 0.018 | 21.260 | 21.263 | 0.016 | 21.490 | 21.486 | 0.018 | 21.700 | 21.702 | 0.011 | 21.910 | 21.912 | 0.011 |
| 0.040 | 11.120 | 11.117 | 0.029 | 11.200 | 11.200 | 0.004 | 11.280 | 11.282 | 0.015 | 11.360 | 11.361 | 0.005 | 11.440 | 11.437 | 0.026 |
| 0.050 | 6.241 | 6.241 | 0.006 | 6.283 | 6.283 | 0.000 | 6.324 | 6.324 | 0.001 | 6.364 | 6.364 | 0.001 | 6.403 | 6.403 | 0.006 |
| 0.060 | 3.907 | 3.907 | 0.007 | 3.930 | 3.930 | 0.010 | 3.953 | 3.953 | 0.008 | 3.976 | 3.976 | 0.010 | 3.997 | 3.997 | 0.006 |
| 0.080 | 1.895 | 1.895 | 0.003 | 1.904 | 1.904 | 0.003 | 1.913 | 1.913 | 0.017 | 1.921 | 1.921 | 0.009 | 1.929 | 1.929 | 0.021 |
| 0.100 | 3.879 | 3.879 | 0.002 | 3.841 | 3.841 | 0.004 | 3.804 | 3.804 | 0.011 | 3.769 | 3.769 | 0.007 | 3.734 | 3.734 | 0.002 |
| 0.150 | 1.430 | 1.430 | 0.002 | 1.416 | 1.416 | 0.005 | 1.403 | 1.403 | 0.034 | 1.389 | 1.389 | 0.027 | 1.377 | 1.377 | 0.028 |
| 0.200 | 0.727 | 0.727 | 0.006 | 0.720 | 0.720 | 0.002 | 0.713 | 0.713 | 0.003 | 0.707 | 0.707 | 0.006 | 0.701 | 0.701 | 0.004 |
| 0.300 | 0.311 | 0.311 | 0.001 | 0.309 | 0.308 | 0.016 | 0.306 | 0.306 | 0.007 | 0.304 | 0.304 | 0.007 | 0.302 | 0.302 | 0.014 |
| 0.400 | 0.190 | 0.189 | 0.016 | 0.188 | 0.188 | 0.022 | 0.187 | 0.187 | 0.008 | 0.186 | 0.186 | 0.024 | 0.185 | 0.185 | 0.021 |
| 0.500 | 0.138 | 0.138 | 0.033 | 0.137 | 0.137 | 0.023 | 0.137 | 0.137 | 0.028 | 0.136 | 0.136 | 0.025 | 0.135 | 0.135 | 0.010 |
| 0.600 | 0.111 | 0.111 | 0.018 | 0.110 | 0.110 | 0.010 | 0.110 | 0.110 | 0.041 | 0.109 | 0.109 | 0.012 | 0.109 | 0.109 | 0.015 |
| 0.800 | 0.083 | 0.083 | 0.001 | 0.083 | 0.083 | 0.001 | 0.082 | 0.082 | 0.001 | 0.082 | 0.082 | 0.003 | 0.082 | 0.082 | 0.001 |
| 1.000 | 0.068 | 0.068 | 0.001 | 0.068 | 0.068 | 0.006 | 0.068 | 0.068 | 0.005 | 0.068 | 0.068 | 0.002 | 0.068 | 0.068 | 0.002 |
| 1.500 | 0.052 | 0.052 | 0.002 | 0.052 | 0.052 | 0.009 | 0.052 | 0.052 | 0.006 | 0.052 | 0.052 | 0.007 | 0.052 | 0.052 | 0.007 |
| 2.000 | 0.045 | 0.045 | 0.004 | 0.045 | 0.045 | 0.010 | 0.045 | 0.045 | 0.005 | 0.045 | 0.045 | 0.003 | 0.045 | 0.045 | 0.005 |
| 3.000 | 0.040 | 0.040 | 0.006 | 0.040 | 0.040 | 0.006 | 0.040 | 0.040 | 0.010 | 0.040 | 0.040 | 0.003 | 0.040 | 0.040 | 0.001 |
| 4.000 | 0.038 | 0.038 | 0.002 | 0.038 | 0.038 | 0.004 | 0.038 | 0.038 | 0.008 | 0.038 | 0.038 | 0.010 | 0.038 | 0.038 | 0.010 |
| 5.000 | 0.038 | 0.038 | 0.011 | 0.038 | 0.038 | 0.004 | 0.038 | 0.038 | 0.001 | 0.038 | 0.038 | 0.005 | 0.038 | 0.038 | 0.009 |
| 6.000 | 0.038 | 0.038 | 0.009 | 0.038 | 0.038 | 0.005 | 0.038 | 0.038 | 0.007 | 0.038 | 0.038 | 0.007 | 0.038 | 0.038 | 0.004 |
| 8.000 | 0.039 | 0.039 | 0.006 | 0.039 | 0.039 | 0.001 | 0.039 | 0.039 | 0.005 | 0.039 | 0.039 | 0.011 | 0.039 | 0.039 | 0.007 |
| 10.000 | 0.041 | 0.041 | 0.011 | 0.041 | 0.041 | 0.005 | 0.041 | 0.041 | 0.003 | 0.041 | 0.041 | 0.011 | 0.041 | 0.041 | 0.004 |
| 15.000 | 0.045 | 0.045 | 0.001 | 0.045 | 0.045 | 0.000 | 0.045 | 0.045 | 0.001 | 0.045 | 0.045 | 0.003 | 0.045 | 0.045 | 0.008 |

Input data procedure for XCOM and Phy-X/PSD. XCOM (NIST): Elemental weight fractions $\{w_j\}$ and photon energies (0.01-15 MeV) were entered in the "Mixture" mode of the NIST XCOM database to obtain photon-interaction cross sections and Mass Attenuation Coefficients (MAC) for each composition [17]. Phy-X/PSD: Using the same elemental composition and energy grid, Phy-X/PSD was used to compute practical shielding/dosimetric indices beyond MAC-LAC (via $\rho_{glass}$), HVL, TVL, MFP, $Z_{eff}$, and $N_{eff}$, across the photon-energy range [18]. Consistency check: MAC trends from Phy-X/PSD were verified to be consistent with XCOM outputs for identical compositions/energies before deriving secondary parameters.

Because the glasses were not fabricated, reported densities are theoretical estimates. Experimental densification, porosity, and thermal history may cause deviations; follow-up synthesis/measurements are planned to validate density and shielding parameters.

## RESULTS AND DISCUSSION

MAC data were obtained using XCOM (NIST) and the Phy-X/PSD platform to evaluate the radiation shielding performance of glass samples (BBTM1-BBTM5) in the energy range of 0.01-15 MeV. The analysis results showed that the largest difference between the XCOM and Phy-X/PSD results was 0.037% (Table 2), indicating a very high accuracy between the two programs. The agreement of the results from the two programs was evaluated using the following formula, as given in Eq. (9).

$$\Delta\,(\%) = \left|\left[\frac{(MAC)_{Xcom} - (MAC)_{Phy-x/PSD}}{(MAC)_{Xcom}}\right]\right| \times 100 \quad (9)$$

MAC is a material property per unit mass and, by definition, does not depend on bulk density; LAC depends on density. Therefore, density changes (e.g., with $MoO_3$ addition) affect LAC, HVL/TVL, and MFP, while MAC variations arise from composition (Z-content, absorption edges) and photon energy [15].

Increasing $MoO_3$ content raises the estimated glass density (Table 1 and Fig. 1), so for a given energy, the LAC and thickness metrics (HVL/TVL/MFP) improve even when MAC remains nearly identical between tools [30]. In this study, the estimated densities increase from 5.666 $g/cm^3$ in the BBTM1 sample to 5.948 $g/cm^3$ in the BBTM5 sample.

Increasing the density of the shielding material improves the quality of the radiation shielding [31]. This is due to the greater number of atoms per unit volume in materials with higher densities, thereby increasing the probability of interaction between radiation and atoms in the material [4].

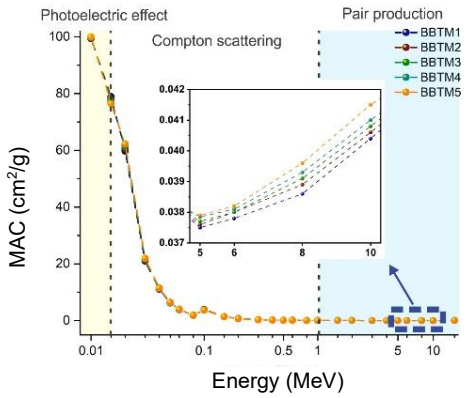


(a)

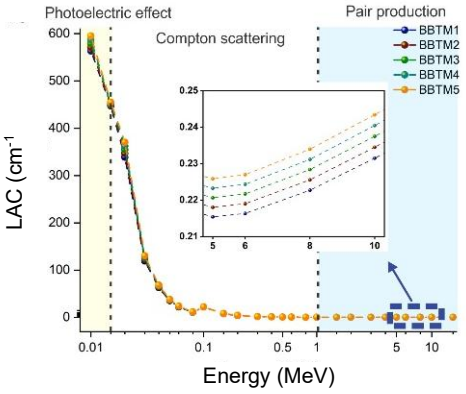


(b)

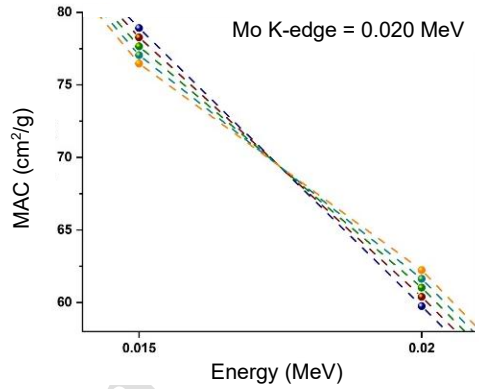


(c)

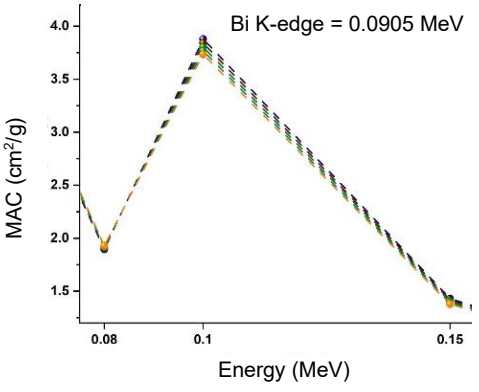


(d)

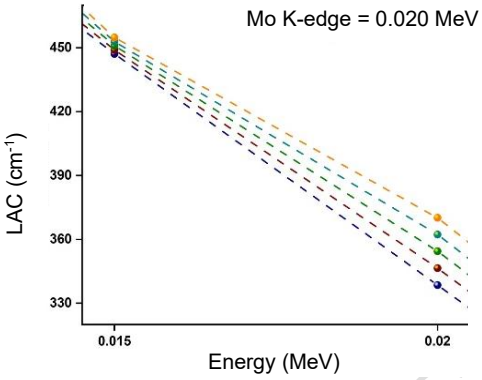


(e)

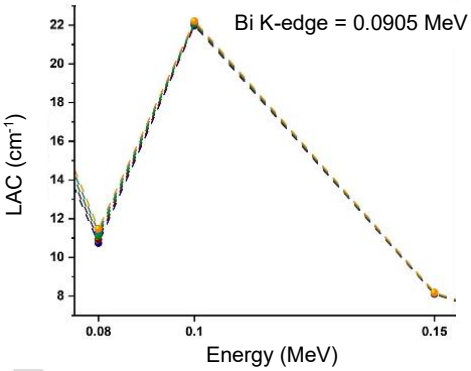


(f)

**Fig. 2.** Attenuation behavior of the studied glasses over 0.010-15 MeV computed with XCOM: (a) MAC; (b) LAC; (c) Zoomed Mo K-edge on MAC; (d) Zoomed Bi K-edge on MAC; (e) Zoomed Mo K-edge on LAC; (f) Zoomed Bi K-edge on LAC.

In general, the higher the incoming radiation energy, the smaller the MAC value of the radiation shielding material [32]. The radiation energy determines the type of interaction between the radiation and the shielding material. In the low energy range (0.010-0.15 MeV), the interaction is dominated by the photoelectric effect, where the radiation interacts with the electrons in the shielding material, and the atom completely absorbs its energy. If the radiation energy exceeds the binding energy of the electrons in the atom, the electrons will be released from their orbits [33]. This interaction significantly reduces the remaining radiation energy, resulting in a sharp decrease in the MAC value graph, as shown in Fig. 2. The photoelectric effect cross section ($\sigma_{pe}$) is influenced by the atomic number (Z) and the radiation energy (E) [4].

At energies around 0.020 MeV, a small increase in the MAC value is observed, which is due to the presence of the molybdenum K absorption edge. An absorption edge is a condition where a material shows a significant increase in radiation absorption at a certain energy. However, in this

study, the contribution of molybdenum to the absorption edge is relatively small due to its non-dominant concentration in the shielding material. In contrast, a significant absorption edge is observed from bismuth (Bi) atoms at an energy of 90.5 keV (in the 0.1 MeV graph) due to the high concentration of bismuth in the sample.

In the medium energy range (0.15-1.02 MeV), the dominant interaction is Compton scattering, where radiation loses some of its energy through interactions with electrons in the material. The decrease in MAC value in this range is not very significant when compared to the decrease that occurs in the photoelectric effect [34]. In the high-energy range (more than 1.02 MeV), the interaction that occurs is pair production; namely, high-energy radiation produces pairs of electrons and positrons. As in Compton scattering, the decrease in MAC value in this range is relatively small [4].

MAC and LAC values show similar trends at an energy of 0.05 MeV. The highest LAC value was recorded in sample BBTM5 at 38.085 $cm^{-1}$, which is higher than that of BBTM1, BBTM2, BBTM3, and BBTM4 at 35.364 $cm^{-1}$, 36.048 $cm^{-1}$, 36.730 $cm^{-1}$, and 37.409 $cm^{-1}$, respectively. The LAC value decreases with increasing radiation energy, but at certain energies, especially at the absorption edge of the material, there is a significant increase. The BBTM5 showed the best performance based on higher MAC and LAC compared to other samples.

The thickness of the radiation shielding material can be evaluated through three main indicators, namely HVL, TVL, and MFP. These three indicators are used to assess the effectiveness of the material in protecting against radiation. The smaller the HVL, TVL, and MFP values, the more effective the material is in protecting against radiation [35]. These three parameters are greatly influenced by the LAC value, where the higher the LAC value, the smaller the HVL, TVL, and MFP values [3,21,22]. In addition, the composition of the shielding material and radiation energy also play an important role in determining the values of these three parameters. Increasing the concentration of $MoO_3$ in the composition of the protective glass has been shown to reduce the HVL, TVL, and MFP values at the same energy. As illustrated in Fig. 3 regarding the HVL and TVL data, at an energy of 1.00 MeV, the HVL value for the BBTM1 sample is 1.789 cm, which is significantly thicker than the HVL value for the BBTM5 sample, which is 1.736 cm.

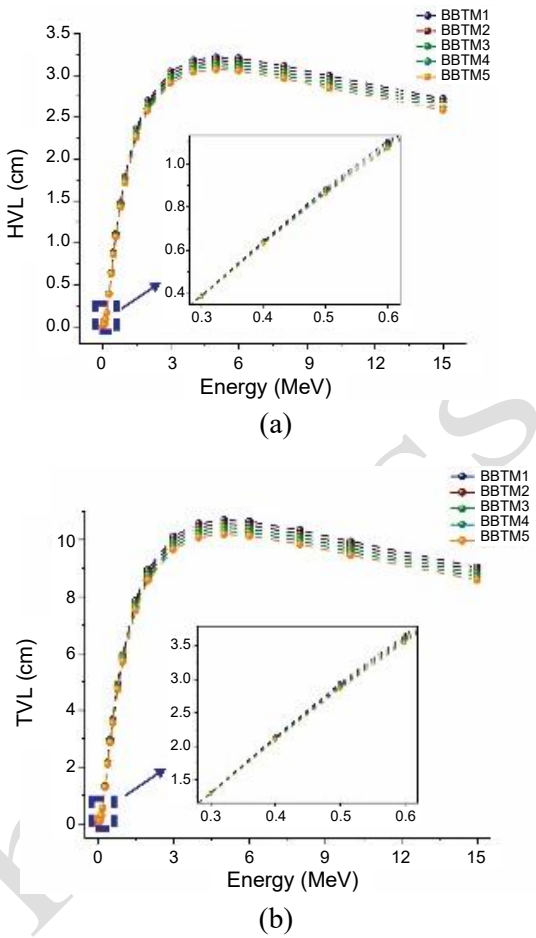


**Fig. 3.** (a) HVL and (b) TVL vs photon energy (0.010-15 MeV) for BBTM1-BBTM5, calculated from XCOM-derived MAC and estimated densities.

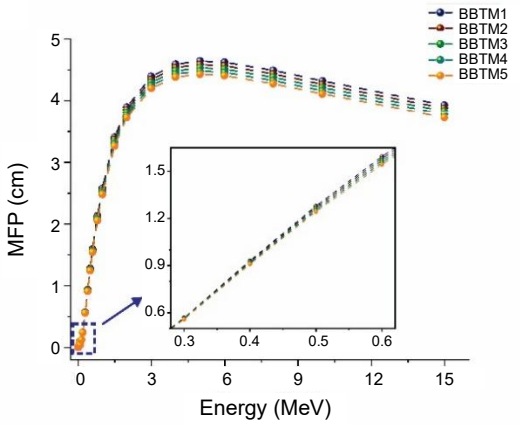


**Fig. 4.** Mean Free Path (MFP) vs photon energy (0.010-15 MeV) for BBTM1-BBTM5, calculated from XCOM-derived MAC and estimated densities.

Based on the three thickness parameters, the results of the study showed that the radiation shielding thickness values followed the order BBTM5<BBTM4<BBTM3<BBTM2<BBTM1. The BBTM5 sample has the best radiation shielding ability compared to other samples. This is due to the higher density of BBTM5, which results in a larger number of atoms per unit volume.

However, in the same sample, increasing radiation energy tends to increase the HVL, TVL, and MFP values, which directly reduces the effectiveness of radiation shielding materials [4]. As shown in Fig. 4, the MFP value at 0.01 MeV energy is 0.002 cm and increases to 3.728 cm at 15 MeV energy. Increasing radiation energy causes a larger number of photons, so the shielding material must have a higher thickness to maintain the same level of protection.

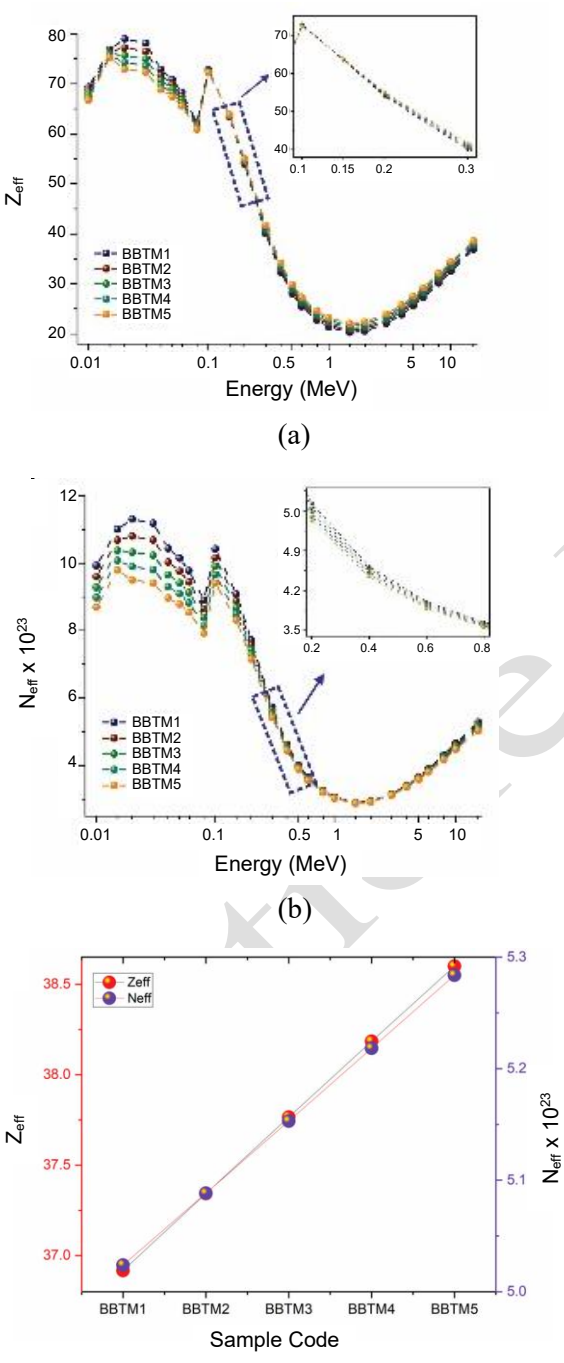


**Fig. 5.** (a) Variation in effective atomic number $Z_{eff}$ and (b) Effective electron density $N_{eff}$ of $MoO_3$-based samples across different energy levels, and (c) The relationship between $Z_{eff}$, $N_{eff}$, and $MoO_3$ concentration at 15 MeV, evaluated using the Phy-X/PSD.

In this study, the glass sample with the highest $MoO_3$ concentration (BBTM5) showed a significant increase in $Z_{eff}$ values at the same energy level. This increase was correlated with the increase in the total number of atoms in the material due to the addition of $MoO_3$, although accompanied by a decrease in atoms originating from $B_2O_3$. Higher $Z_{eff}$ values are directly related to better radiation shielding effectiveness [23,24], as shown in Fig. 5(a). $Z_{eff}$ values fluctuate in the following ranges: 69.38-36.92 (BBTM1), 68.68-37.34 (BBTM2), 68.01-37.77 (BBTM3), 67.38-38.18 (BBTM4), and 66.77-38.60 (BBTM5). In the same sample, the $Z_{eff}$ value tended to decrease with increasing radiation energy. However, at the absorption edges of the constituent metals, such as the K absorption edges of Bi and Mo, there is a significant increase in the $Z_{eff}$ value.

The $N_{eff}$ values of all samples are in the following ranges: $9.93 \times 10^{23}$ - $5.28 \times 10^{23}$ (BBTM1), $9.60 \times 10^{23}$ - $5.22 \times 10^{23}$ (BBTM2), $9.28 \times 10^{23}$ - $5.15 \times 10^{23}$ (BBTM3), $8.98 \times 10^{23}$ - $5.09 \times 10^{23}$ (BBTM4), and $8.69 \times 10^{23}$ - $5.02 \times 10^{23}$ (BBTM5), as shown in Fig. 5(b). The discontinuity of the $N_{eff}$ results is also seen in the K absorption edges of Bi and Mo, which is consistent with the pattern observed in $Z_{eff}$. Fig. 5(c) shows the variation of $Z_{eff}$ and $N_{eff}$ values of all samples at the highest energy, which is 15 MeV. From the graph, it can be observed that the highest $Z_{eff}$ and $N_{eff}$ values were recorded in the BBTM5 sample. Based on these results, it can be concluded that the BBTM5 sample has the highest radiation shielding ability among the five samples analyzed.

The lower the TF value, the better the quality of the radiation shielding material. The TF value is influenced by the radiation energy, the thickness of the shielding material, and its composition. In this study, the TF value was calculated at various thicknesses of the protective glass (0.5-3 cm) by considering the radiation energy of certain radioisotopes (0.662 MeV, 1.173 MeV, 1.332 MeV, and 2.506 MeV). As in Fig. 6, the results show that the higher the radiation energy and the thinner the shielding material, the more photons are able to pass through the material, so the TF value increases. In the same sample, such as BBTM5, the TF value shows an increase with increasing radiation energy.

The composition of this glass shield is influenced by the presence of $MoO_3$, which significantly increases the density of the material. This increase in density reduces the number of photons that successfully pass through the material, resulting in a lower TF value [36]. Based on the results of the study, the BBTM5 sample proved to be the most effective radiation shielding material compared to other samples. The presence of $MoO_3$ greatly contributes to increasing the effectiveness of the radiation shield by reducing the photon transmission rate. Thus, the BBTM5 sample shows optimal performance in preventing photon transmission through the shielding material.

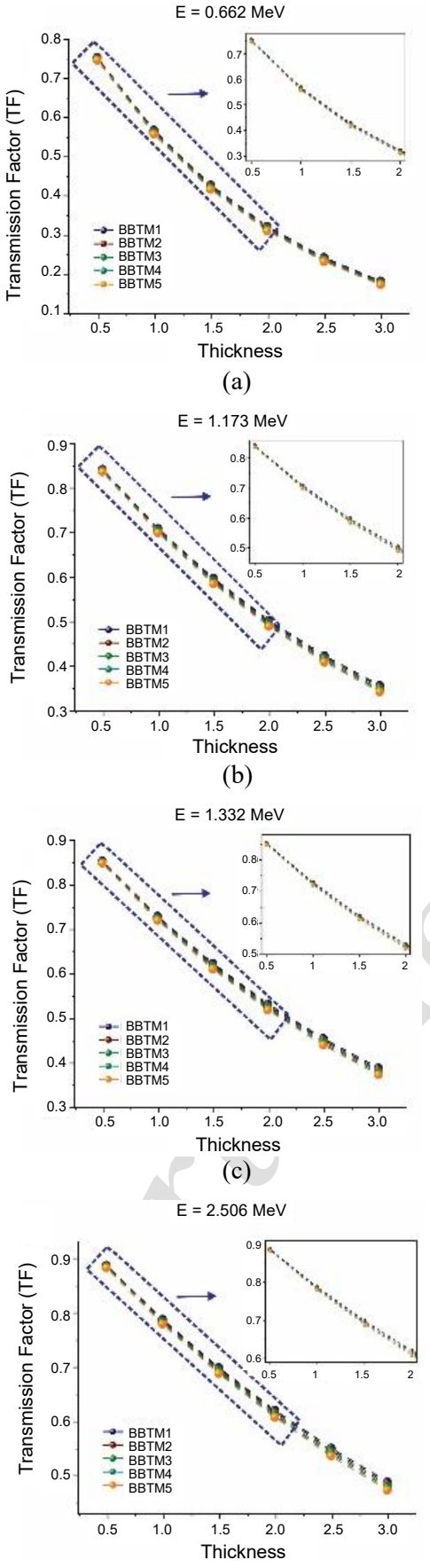


**Fig. 6.** Transmission Factor (TF) at four photon energies representative of radioisotopes (0.662, 1.173, 1.332, 2.506 MeV) for glass thicknesses 0.5-3.0 cm, calculated from XCOM-derived LAC.

This study shows that the addition of $MoO_3$ into bismuth boro-tellurite glass significantly enhances the effectiveness of the material as a radiation shield in the energy range of 0.01-15 MeV. Among all the samples tested, BBTM5 showed the best performance. This is due to the high concentration of $MoO_3$ in its composition compared to other samples. This finding is consistent with previous studies, which also revealed that increasing the $MoO_3$ content in radiation-shielding materials significantly enhances their protective performance [37,38].

## CONCLUSION

The gamma-ray shielding of glass samples with the composition $(50\text{-}x)B_2O_3\text{-}10TeO_2\text{-}30Bi_2O_3\text{-}10Li_2O\text{-}xMoO_3$ has been theoretically analyzed using XCOM software from NIST and Phy-X/PSD. This study includes the analysis of the main parameters of radiation shielding, such as MAC, LAC, HVL, TVL, MFP, $Z_{eff}$, $N_{eff}$, and TF in the energy range of 0.010-15 MeV. The addition of $MoO_3$ concentration and photon energy has a significant effect on these parameters. At an energy of 0.020 MeV, the BBTM5 glass sample, which has the highest $MoO_3$ concentration, shows the highest attenuation coefficient, namely MAC of 62.230 $cm^2/g$ and LAC of 270.120 $cm^{-1}$. Validation of the MAC calculation shows a high degree of agreement between the results of the two software used, confirming the accuracy of the applied theoretical method. Increasing the concentration of MoO3 also increased the radiation shielding effectiveness, as reflected by the decrease in HVL, TVL, and MFP values in the order BBTM5 < BBTM4 < BBTM3 < BBTM2 < BBTM1 in the entire energy range. The results showed that BBTM5 had the best gamma radiation shielding ability in the energy range of 0.010-15 MeV. These findings provide a strong basis for the development of better glass compositions in the future, enabling the application of this material to a wider spectrum of energy and radiation types. Although this study yielded significant and promising findings, there are some limitations, such as the lack of experimental data and a limited sample size. Further research is needed with larger sample sizes and exploration of wider $MoO_3$ concentrations to improve the reliability and feasibility of this material in real applications.

## ACKNOWLEDGMENT

The authors gratefully acknowledge the Department of Physics, Faculty of Science and

Mathematics, Diponegoro University, for a supportive research environment and access to essential facilities. This work was funded by Diponegoro University through the Riset Publikasi Internasional (RPI) research scheme under contract number 222-532/UN7.D2/PP/IV/2025. We also thank the Institute for Research and Community Services (LPPM UNDIP) for their valuable support throughout the project.

## AUTHOR CONTRIBUTION

Oki Ade Putra contributed to writing original draft and writing review & editing; Rin Hafsahtul Asiah to formal analysis, methodology, and resources; Heri Sutanto to validation and supervision; Suci Faniandari to resources and writing-review & editing; and Erik Bhekti Yutomo to validation and project administration.

## REFERENCES

1. I. N. Fathy, A. A. El-Sayed, M. E. Elfakharany *et al.*, Nucl. Eng. Des. **429** (2024) 113626.
2. G. Tyagi, A. Singhal, S. Routroy *et al*., Mater. Today Proc. **32** (2020) 746.
3. Y. Hou, M. Li, Y. Gu *et al.*, Polym. Compos. **39** (2018) E2106.
4. A. H. Alsaab and S. Zeghib, Polymers **15** (2023) 2142.
5. O. A. Putra, D. N. I. Saputra, and F. B. Arafat, Radiat. Eff. Defects Solids (2025) 1.
6. A. M. El-Khayatt, A. A. Alghamdi, A. Sabik *et al.*, Ann. Nucl. Energy **205** (2024) 110576.
7. M. S. Ali, A. M. Abdelmonem, S. K. Elshamndy *et al*., Atom Indones. **48** (2022) 237.
8. A. Maatouk, R. M. Almotawa, S. A. Alshehri *et al.*, Radiat. Phys. Chem. **225** (2024) 112142.
9. M. Al Huwayz, B. Basha, A. Alalawi *et al*., J. Radiat. Res. Appl. Sci. **17** (2024) 101119.
10. A. H. Almuqrin, M. I. Sayyed, F. F. Alharbi *et al.,* Opt. Mater. **157** (2024) 116213.
11. M. Bengisu, J. Mater. Sci. **51** (2016) 2199.
12. N. A. M. Alsaif, M. Alotiby, M. Y. Hanfi *et al*., J. Aust. Ceram. Soc. **57** (2021) 1267.
13. S. Yin, H. Wang, S. Wang *et al.*, Crystals **12** (2022) 178.
14. J. S. Alzahrani, T. Kavas, R. Kurtulus *et al*., J. Mater. Sci. Mater. Electron. **32** (2021) 18994.
15. S. M. Ngaram, S. Hashim, M. S. M. Sanusi *et al*., Radiat. Phys. Chem. **226** (2025) 112355.
16. M. S. Al-Buriahi, E. O. Echeweozo, C. Sriwunkum *et al*., Nucl. Eng. Technol. **57** (2024) 103313.
17. M. J. Berger, J. H. Hubbell, S. M. Seltzer *et al*., XCOM: Photon Cross Sections Database. National Institute of Standards and Technology, Gaithersburg (2010).
18. E. Şakar, Ö. F. Özpolat, B. Alım *et al.*, Radiat. Phys. Chem. **166** (2020) 108496.
19. E. Hannachi, M. I. Sayyed, Y. Slimani *et al.*, Inorg. Chem. Commun. **169** (2024) 112996.
20. N. Alomayrah, M. M. Albarqi, R. A. Alsulami, *et al.,* Results Phys. **58** (2024) 107441.
21. D. I. Tishkevich, A. A. Rotkovich, S. A. German *et al*., RSC Adv. **13** (2023) 24491.
22. S. N. Ahmed, *Interaction of Radiation with Matter,* in: Physics and Engineering of Radiation Detection (Second Edition), Elsevier, Amsterdam (2015) 65.
23. E. Şakar, Ö. F. Özpolat, B. Alım *et al*., Radiat. Phys. Chem. **166** (2020) 108496.
24. G. Hoşgör, E. Tabar, E. Kemah *et al.*, Radiat. Phys. Chem. **226** (2025) 112281.
25. A. H. Alomari and S. M. Al-Qahtani, J. Radiat. Res. Appl. Sci. **17** (2024) 100996.
26. G. ALMisned, G. Susoy, H. M. H. Zakaly *et al.,* Open Chem. **21** (2023) 20220354.
27. J. D. Vienna, A. Fluegel, D. S. Kim *et al*., Glass Property Data and Models for Estimating High-Level Waste Glass Volume, Pacific Northwest National Laboratory (PNNL), Richland (2009).
28. J. D. Vienna, A. Heredia-Langner, S. K. Cooley *et al*., Glass Property-Composition Models for Support of Hanford WTP LAW Facility Operation, Pacific Northwest National Laboratory (PNNL), Richland (2022).
29. A. H. Alomari and S. M. Al-Qahtani, J. Radiat. Res. Appl. Sci. **17** (2024) 100996.
30. A. H. Almuqrin, M. I. Sayyed, M. U. Khandaker *et al*., Radiat. Phys. Chem. **220** (2024) 111629.
31. A. Fisli, E. Yulianti, B. Hanurajie *et al*., Atom Indones. **1** (2023) 45.

32. P. G. Ghule, G. T. Bholane, R. P. Joshi *et al*., Radiat. Phys. Chem. **216** (2024) 111452.

33. M. F. L'Annunziata, *The Atomic Nucleus, Nuclear Radiation, and the Interaction of Radiation with Matter,* in: Handbook of Radioactivity Analysis, Elsevier, London (2020) 1.

34. O. Kilicoglu, C. V. More, F. Akman *et al*., Radiat. Phys. Chem. **194** (2022) 110039.

35. M. R. Ambika, N. Nagaiah, V. Harish *et al*., Radiat. Phys. Chem. **130** (2017) 351.

36. M. T. Alresheedi, M. Elsafi, Y. T. Aladadi *et al.*, Polymers **15** (2023) 2160.

37. R. U. Singh, K. C. Sekhar, J. S. Alzahrani *et al*., Ceram. Int. **49** (2023) 11600.

38. A. Saleh, N. A. Harqani, W. Al-Ghamdi *et al*., Mater. Chem. Phys. **322** (2024) 129574.